Available online at www.sciencedirect.com

SciVerse ScienceDirect

Journal of the European Ceramic Society 32 (2012) 1561–1573

www.elsevier.com/locate/jeurceramsoc

Tailoring of functionally graded zirconia–mullite/alumina ceramics

Emad M.M. Ewais [a,*], Dina Hussien Amin Besisa [a], Zaki Ismail Zaki [a], Abd El Hakim Taha Kandil [b]

[a] *Refarctory & Ceramic Materials Division (RCMD), Advanced Materials Department, Central Metallurgical R&D Institute (CMRDI), P.O. Box 87, Helwan, 11421 Cairo, Egypt*

[b] *Chemistry Department, Faculty of Science, Helwan University, Egypt*

Received 14 August 2011; received in revised form 22 November 2011; accepted 16 January 2012
Available online 16 February 2012

Abstract

A new tailored zirconia–mullite/(0–100 vol%) alumina as functionally graded ceramics (FGCs) was designed and synthesized by reaction sintering of zircon and alumina. Zircon and alumina powder mixtures were mixed, stacked, compacted in a cylindrical die and sintered. The sintered samples made of 11 layers and varied gradually in composition by 10 vol% from one layer to the other layer (i.e. from zirconia–mullite layer to alumina layer) resulted in continuous functionally graded ceramics without sharp interfaces. Phase composition and densification behaviors of the samples were investigated. Microstructure, mechanical and thermal properties of FGC and its non-layered composites were studied. Results showed that the tailored FGZM/A gave continuous homogenous structure with highly improved physical, mechanical and thermal properties. The different properties of tailored FGZM/A recorded average values or rather better of its non-layered composites which gave a new way for material design.

Keywords: FGZM/A; Sintering; Microstructure; Mechanical properties; Thermal properties

1. Introduction

Recent advances in materials processing and engineering, and the continual need for new materials with tailored properties and different functions at different sides have led to a new class of graded materials that has been long established in nature. These graded materials are seen in bio-tissues of plants, animals and in our human bodies. Bones and teeth, bamboos, shells and coconut leaves are good examples, which are very strong near outside surface and soft and tough inside.[1] Such graded materials are referred to as functionally graded materials (FGMs). FGMs are multi-layered composites in which its composition and/or functions are varying continuously or step-wisely from one side to the other side, leading to gradual change in materials properties. The irreconcilable properties at each side of FGM can be fully utilized. FGM can be tailored according to the application requirements by controlling the suitable components to achieve some specific tailored applications and overcome the problems of laminated composites.[2] FGM are widely used in many expanding fields such as biomedical, tribological, aerospace, microelectronics, military and nuclear applications.[3–6] In the past, FGMs compositions included at least one metal phase, but recently great attention has been devoted to functionally graded ceramics–ceramics and glass–ceramics system due to their attractive properties.[2]

Zirconia–mullite/alumina in the ZrO_2–SiO_2–Al_2O_3 system is one of the important ceramic composite system.[7] Mullite has high melting point, chemical stability, low thermal expansion and thermal conductivity, attractive bending strength at high temperature, low creep rate and excellent thermal shock resistance.[8–12] However, the low fracture toughness and relatively low strength at room temperature of mullite compared with other engineering material and the difficulties in obtaining fully dense object hinder its wide scale applications.[13] Alumina also has favorable properties as high hardness, high wear resistance and resistance to corrosion by chemical reagents and thermodynamic stability. However it suffers from low strength and low fracture toughness. Also alumina experiences grain growth during sintering that causes several disadvantages for its single phase application including porosity and abnormal grain growth. On the other hand, ZrO_2 based composites have occupied a special place in the list of the most promising ceramics that can be produced on a large scale.[7] It has superior physical and mechanical properties, high melting temperature, chemical and corrosion

* Corresponding author.
E-mail address: dr_ewais@hotmail.com (E.M.M. Ewais).

0955-2219/$ – see front matter © 2012 Elsevier Ltd. All rights reserved.
doi:10.1016/j.jeurceramsoc.2012.01.016

resistance to temperature above the melting point of alumina, low thermal conductivity (20% that of alumina) and temperature capability up to 2400 °C. Its fracture toughness is high and it is slightly wetted by siliceous and metallic melt compared with mullite. These superior advantages of zirconia enable it to be used in high temperature engineering applications and can be added to a large number of ceramic materials to improve their mechanical properties including mullite and alumina through t-m phase transformation.[14–16] Several studies have been carried out on the systems alumina/zirconia,[17–21] mullite/zirconia[22–29] and mullite/alumina.[30–36] These studies have shown the effect of zirconia dispersion on sinterability and improving the mechanical properties of alumina and mullite. However, very few published works have been discussed alumina–mullite–zirconia system composites. Alumina–mullite–zirconia (AMZ) refractories are widely used in the forehearth, distributor, feeders and glass melting furnaces as well as plungers, spouts, tubes, stirrers, channels, rotor segments, mantle block and orifice rings.[30,32] The wide spread usage of this class of material is due to their high temperature corrosion resistance and unique microstructural features, including the inter-locking of alumina crystals and the glassy matrix with the almost insoluble zirconia crystals.[37,38] AMZ refractory ceramic is reported to have better thermal shock resistance and high thermal and mechanical properties than zirconia/mullite and alumina/mullite and even than pure mullite ceramic systems.[24,31,39] To the best of our knowledge, no available works discussed the tailoring of functionally graded material from these composite components. Tailored functionally graded zirconia–mullite/alumina is expected to minimize the mismatch gradually in thermal expansion coefficient among the layers and the components of each layer, improve the mechanical properties and sinterability of both mullite and alumina to be used as new advanced applications required two external surfaces with different composition, functions and graded properties. This new tailored material is expected to combine the excellent properties of alumina (high refractoriness, hardness, and wear resistance), mullite (high creep resistance, low thermal expansion coefficient, excellent thermal shock resistance and attractive bending strength at high temperature) and that of zirconia (high fracture toughness, strength, corrosion resistance and low thermal conductivity).

In the present work, eleven-layer of functionally graded zirconia–mullite/(0–100 vol%) alumina with increment 10 vol% from layer to the other were tailored based on reaction sintering. As a parallel work, the eleven layers constituted FGM were tailored as non-layered separated composites by the same technique to follow the change of material properties as a function of change in material composition. The effect of different alumina particle sizes and sintering conditions as controlling factors of reaction completion and densification was studied. Physical, mechanical and thermal properties and microstructure of the tailored functionally graded zirconia–mullite/alumina and its non-layered separated composites constituted it were evaluated.

Table 1
Particle size distribution of alumina and zircon powders.

	Different alumina particle size, μm			zircon
	I	II	III	
d_{50}	2.5	18.80	55.2	1.16
d_{90}	20	40.44	113.9	3.16

Table 2
Chemical composition analysis of alumina and zircon starting powders as measured by XRF.

Oxides	Chemical composition, wt%	
	Zircon	Al_2O_3
SiO_2	32.60	0.24
Al_2O_3	–	99.36
ZrO_2	66.95	–
TiO_2	0.20	–
Fe_2O_3	0.19	0.03
CaO	–	0.07
Na_2O	0.05	0.30

2. Experimental procedure

2.1. Starting materials

High purity $ZrSiO_4$ powder (99.5%) having a mean particle size (d_{50}) of 1.16 μm was used as a starting material. It was provided by El-Nasr Company for Refractories and Ceramics, Sornaga, Egypt. Pure Al_2O_3 powder (>99%) was supplied by Arabic Scientific office, Egypt. Alumina with a mean particle sizes (d_{50}) of 2.5 μm, 18.8 μm and 55.2 μm were used. The particle size of alumina and zircon characterized by d_{50} and d_{90} are given in Table 1. The Particle size distribution of zircon and alumina was measured using a laser light-scattering particle-size analyzer (Model LB500, Horiba, Tokyo). The chemical analysis of alumina and zircon powders supported by Panalytical XRF (Model advanced axios, Netherlands) is given in Table 2.

2.2. Design and sintering

Functionally graded zirconia–mullite/alumina (FGZM/A) and its constituent eleven composites were tailored based on reaction sintering of zircon and alumina with different ratio in each composite layer and according to equation (1). Table 3 lists the alumina, zirconia and mullite contents that were calculated by equation (1) for each composite in vol% and wt%. This Table also shows the amounts of zircon and alumina required in each composite.

$$2ZrSiO_4 + (3 + X)Al_2O_3 = 2ZrO_2 + 3Al_2O_3{\cdot}2SiO_2 + XAl_2O_3 \quad (1)$$

X is the amount of alumina increased by 10 vol% from layer to layer in the tailored FGZM/A.

Zircon and alumina powders with their different ratio in each composite layer were mixed separately in a slow rotating mill with alumina ball for 2 h using ethanol as mixing medium to ensure high homogeneity. The obtained slurries

Table 3
Amounts of alumina and zircon used to produce each composite and concentration of A, Z and M after sintering.

Composite layer number	Composition, wt%		Experimental phases, wt% (vol%)		
	Al_2O_3	$ZrSiO_4$	XAl_2O_3	ZrO_2	Mullite
1	45.5	54.5	0 (0)	36.65 (26)	63.34 (74)
2	52	48	11.89 (10)	32.29 (23)	55.81 (67)
3	58.16	41.84	23.27 (20)	28.125 (21)	48.6 (59)
4	64.1	35.9	34.21 (30)	24.11 (18)	41.66 (52)
5	69.86	30.13	44.79 (40)	20.23 (16)	34.97 (44)
6	75.53	24.66	54.81 (50)	16.56 (13)	28.62 (37)
7	80.633	19.36	64.53 (60)	12.99 (10)	22.46 (30)
8	85.76	14.23	73.93 (70)	9.55 (8)	16.51 (22)
9	90.66	9.33	82.91 (80)	6.26 (5)	10.82 (15)
10	95.4	4.6	91.61 (90)	3.07 (3)	5.31 (7)
11	100	0	100	0	0

were dried at 115 °C overnight. The FGZM/A samples were successively stacked manually layer by layer in a cylindrical steel die. Boron nitride lubricant was used each time around the contact surface of the die for smooth application of force and release of the compacted samples. Both separated composites (non-FGZM/A) and FGZM/A samples were pressed under pressure of 78 Mpa using uni-axial press (Mega 30t-KPD-10A, Spain). The compaction load was maintained for 1 min to achieve uniform distribution of the pressure throughout the compacts. Finally eleven green compacted composites in a cylindrical shape with (6–7 mm for composite and 12–13 mm for FGC) height and (12 mm) in diameter were produced. Both of separated pressed zirconia–mullite/alumina composites and FGZM/A targeted structure were sintered in a programmable electric furnace (Nabertherm-max 1800 C, Germany) at two different sintering regimes at 1550 and 1650 °C. The temperature of the samples was kept constant at a rate of 5 °C/min from room temperature up to the maximum firing temperature, and sintered for different times 2, 4 and 6 h. The eleven layered functionally graded zirconia–mullite/alumina designation is shown in Fig. 1. This figure illustrates the form of the proposed FGZM/A which consists of 11 layers; nine of them are zirconia–mullite/alumina composites with different graded compositions while the two outer surfaces are zirconia–mullite and alumina.

2.3. Testing and characterization

2.3.1. Mineral composition and densification parameters

Phase composition and crystalline phases in different layers of the FGZM/A were identified by advanced X-ray powder diffraction using a Brukur advanced X-ray diffractometer model D8 Kristalloflex (Ni-filtered Cu Kα radiation; λ = 1.544 Å). The X-ray diffractometer was attached with semi-quantitative measurements to follow up the reaction sequence and phase content in each layer. Densification parameters in term of apparent porosity and bulk density of sintered FGZM/A and non-layered composites were determined by Archimedes immersion technique using distilled water **ASTM C 373-72, 1984**.[40] The linear shrinkage of both separated and functionally graded zirconia–mullite/alumina was calculated by determining the diameter of specimens before and after sintering.

2.3.2. Microstructure investigation

Microstructural characterization was conducted to study the distribution of ceramic components in each composite layer, nature of interfacial bonding between each two adjacent layers and surface morphology. The obtained microstructures of the different composites and different positions in the FGZM/A were examined by using various techniques. Optical polarizing microscopy (Nikon-EPIPHOT 300, Japan) was used for the investigation of the FGZM/A graded interfaces and Scanning electron microscopy (SEM; Model JSM-5410, JEOL, Tokyo) was used for microstructure investigation.

2.3.3. Mechanical properties

Macrohardness and fracture toughness of the FGZM/A and its separated composites have been determined using Vickers

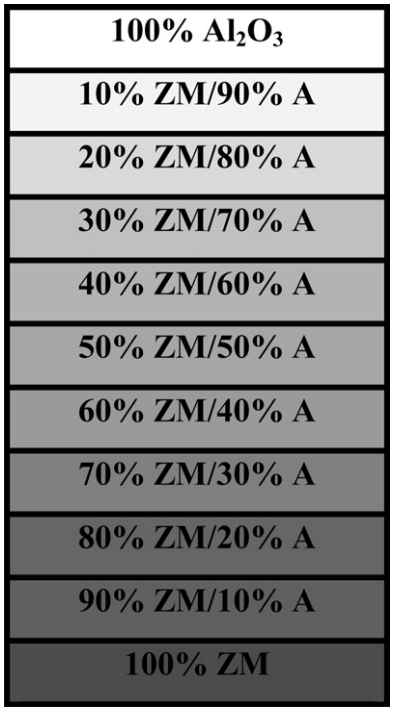

Fig. 1. Composition distribution model of the functionally graded zirconia–mullite/alumina.

indentation method[41–50] with load of 30 kg for 15 s. Vickers hardness was computed using the following relation:

$$\mathrm{Hv} = 0.0018544\frac{p}{d^2}$$

where p is the indentation load (N), d is average length of the two diagonals of the indentation (mm). Hv is the Vickers hardness in unit of (GPa).

Fracture toughness "K_{IC}" was calculated based on the nature of cracks observed. Cracks produced via Vickers indentation have been divided into two systems, Palmquist and half-penny cracks. Palmquist cracks are characteristic of materials having high fracture toughness value.[51–53] K_{IC} based on the Palmquist crack model was calculated using the following relation:

$$K_{IC} = 0.0515\frac{p}{c^{3/2}}$$

However, halfpenny cracks resemble materials which have low toughness values.[51–53] K_{IC} based on the half-penny crack model was calculated using the following relation:

$$K_{IC} = 0.0726\frac{p}{c^{3/2}}$$

where c is the crack length measured from the middle of the Vickers indentation (m). P is the indentation load (N). K_{IC} is the fracture toughness (MPa $m^{0.5}$).

Cold crushing strength was measured according to **ASTM C 1424-04, 2006**.[54]

2.3.4. Thermal properties

Linear thermal expansion (LTE) and its coefficient (CTE) of the tailored separated composites (non-layered) and FGZM/A were measured according to **ASTM C 372-94, 2001**.[55] This test was performed using dilatometery (Linseis Inc., Germany, Model L76/1550) in the temperature range of room temperature up to 1200 °C with a heating rate and cooling rate of 10 °C/min.

The sintered FGZM/A and its separated individual composites were subjected to thermal shocks by heating to 1000 °C and then quenched into water at 20 °C. This test was conducted according to PRE/R5 standard, 1987.[56] After 30 cycles of thermal shock, microscopic examination of the samples was done to determine damage/distortions developed on surface or subsurface regions. The macrohardness and microstructure were studied after thermal shock treatment and compared with the results from untested sample data.

3. Results and discussion

3.1. Processing of targeted ZM composite

The tailoring of zirconia–mullite/alumina composite in each layer of the functionally graded structure is divided into two steps; reaction and sintering of zircon and alumina which may be take place as a simultaneous process as in hot pressing and presureless sintering at 1450 °C[57] or as separated steps.[58]

In this work, zircon dissociates to yield amorphous SiO_2 on heating. The amorphous SiO_2 softens with an increase in temperature and starts to dissolve alumina to aluminosilicate glass.

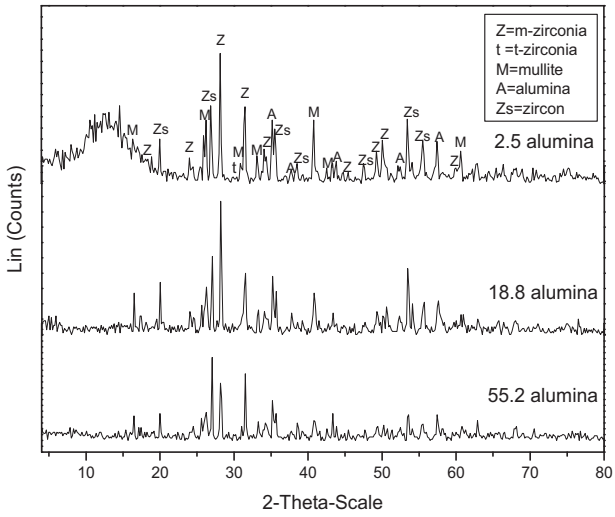

Fig. 2. XRD pattern of targeted ZM composite sintered at 1550 °C/2 h using different mean particle sizes of alumina.

Nucleation of mullite takes place after exceeding the critical concentration of alumina in the glass phase.[23] This reaction is accompanied by a densification process. In the light of this concept, particle sizes, sintering temperature and time were taken as criterion for determination of the optimum condition of tailoring of FGZM/A.

3.1.1. Mineral composition and densification parameters

3.1.1.1. Effect of alumina particle size. Fig. 2 shows XRD patterns of targeted ZM composite sintered at 1550 °C/2 h using different alumina particle sizes. The patterns indicate that unreacted zircon and alumina phases are detected with all alumina particle sizes used. By reducing the particle size of alumina from 55.2 to 2.5 μm, the amount of zircon and alumina decrease and the intensity of zirconia and mullite phases increase. For 2.5 μm alumina, a hump is revealed as an indicator for the formation of amorphous SiO_2. This means that the reaction can proceed forward to the products (ZrO_2 and mullite) if the firing temperature is increased. Therefore, the decrease of alumina grain size lead to a significant effect on the reaction between alumina and zircon, but the reaction did not reach to completion with the appearance of free alumina and zircon. This implies that either sintering temperature (1550 °C) and/or sintering time (2 h) are not sufficient.

3.1.1.2. Effect of sintering conditions. The targeted ZM mixture using the effective particle size of alumina (2.5 μm) is fired at 1650 °C with varying times (2, 4 and 6 h). As shown in X-ray patterns, Fig. 3, the increase of the sintering temperature to 1650 °C/2 h led to complete disappearance of zircon and decrease of alumina peak intensity. However, with the increase of the sintering time to 4 and 6 h at the same temperature (1650 °C), alumina completely vanished. Based on these outputs, Optimum conditions concluded for complete conversion of zircon and alumina into targeted ZM composite (100%) are 1650 °C for 6 h.

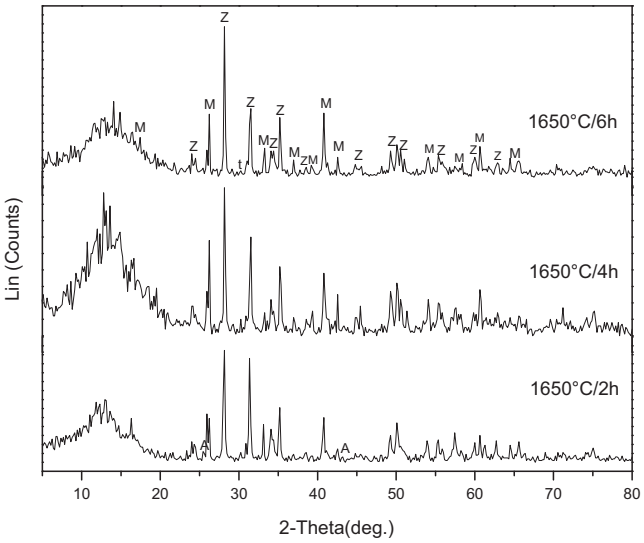

Fig. 3. XRD pattern of targeted ZM composite sintered at 1650 °C at different sintering time.

Generally, densification parameters in terms of apparent porosity, bulk density and linear shrinkage are significantly influenced by the reaction. In this work, the densification parameters of the targeted ZM composite are reached to its maxima at 1650 °C/6 h. The use of alumina particle size of 2.5 μm, sintering temperature of 1650 °C and increasing the sintering time to 6 h, the apparent porosity of targeted ZM composite decreased to 1.35% and bulk density and linear shrinkage increased to 3.44 g/cm^3 and 14.33% respectively. These results are in good agreement with the general principles; apparent porosity is inversely proportional with the bulk density and linear shrinkage. The improvement in densification parameters reflects the completion of reaction between zircon and alumina. This means that the reaction is accompanied by a densification process, i.e. the reaction densification is conducted by thermal activation. Based on mineral composition and densification parameters, the most suitable conditions for achieving the targeted ZM composite and the different non-layered ZM/A composites is using alumina with 2.5 μm grain size and sintering at 1650 °C/6 h.

3.2. Processing of FGZM/A and its non-layered composites

3.2.1. Densification parameters

Apparent porosity, bulk density and linear shrinkage of FGZM/A and its different non-layered composites sintered at 1650 °C for 6 h are given in Table 4. The apparent porosity of ZM composite (100%) is lower than that of the other next layers which have different amounts of alumina. It started to increase in layer-2 (10% alumina). After which a slight decrease in porosity is noticed up to layer-6 (50% alumina). From layer-6 to layer-10 (90% alumina) a significant and gradual decrease in apparent porosity is noticed. Finally, the apparent porosity increased again in layer-11 (100% alumina). This behavior can be attributed to the following:

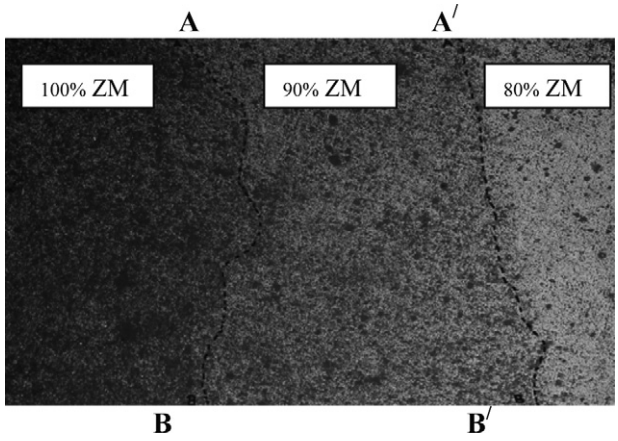

Fig. 4. Micrograph of interfaces between two layers in FGZM/A showing interface (AB) between first and second and (A′B′) interface between second and third layers.

- The gradual increase of alumina from layer to layer decreased the apparent porosity due to the fact that alumina is denser than mullite and addition of fine grained alumina causes a significant reduction in porosity through liquid phase sintering which fills the interparticle voids.[39]
- Exaggerated abnormal grain growth relative to alumina single phase causes several disadvantages.[59] This can explain the increased porosity of the batch composed of 100% alumina.

In multilayered specimens as reported,[60] the interfaces with discontinuity in composition provide an additional source of pore formation. However, in this case, a lower value of the apparent porosity of FGZM/A compared by the average porosity of its entire individual composite layers was recorded, see Table 4. This can be explained by the formation of strong interfacial bonding between each two consecutive layers. Based on these results, FGZM/A tailored by layering of large numbers of graded ZM/A composites overcome the shortcomings from the interfacial bonding mismatch and expected to have a good thermal stability during subsequent thermomechanical loading. In addition, it can be offered as a candidate of new advanced applications.

3.2.2. Microstructure

Optical micrograph of polished surface of the functionally graded zirconia–mullite/alumina sintered at 1650 °C/6 h is illustrated in Fig. 4. This figure shows the microstructure of interfacial region between ZM, ZM/(10%)A and ZM/(20%)A layers. 100 zirconia–mullite/90 alumina and 90/80 composition layers. A dotted line (AB) and (A′B′) mark the interface between two adjacent layers. No sharp interfaces are formed and there is no residual porosity observed on the layer interface. In general, all interfaces are characterized by a smooth transition in microstructure from one layer to the other. There are some wavy lines indicating the non-uniformity in the layer thickness as powders placed in the die manually during compaction.

The scanning electron microscope (SEM) observations of the eleven non-layered ZM/A sintered composites are illustrated in Fig. 5. These micrographs show a gradual compositional

Table 4
Apparent porosity, bulk density and linear shrinkage of separated non-layered zirconia–mullite/alumina composites and FGZM/A sintered at 1650 °C/6 h.

Layer number	Al_2O_3 vol%	Apparent porosity, %	Bulk density, g/cm^3	Linear shrinkage, %
1	0	1.71	3.43	14.33
2	10	10.52	3.22	13.96
3	20	8.71	3.28	14.47
4	30	8.49	3.34	14.88
5	40	8.24	3.39	16.21
6	50	7.51	3.44	16.99
7	60	5.55	3.55	18.44
8	70	3.24	3.64	18.58
9	80	0.81	3.74	20.94
10	90	0.40	3.75	20.96
11	100	3.84	3.60	20.62
Average	–	5.31	3.48	17.30
FGZM/A	–	5.04	3.49	17.22

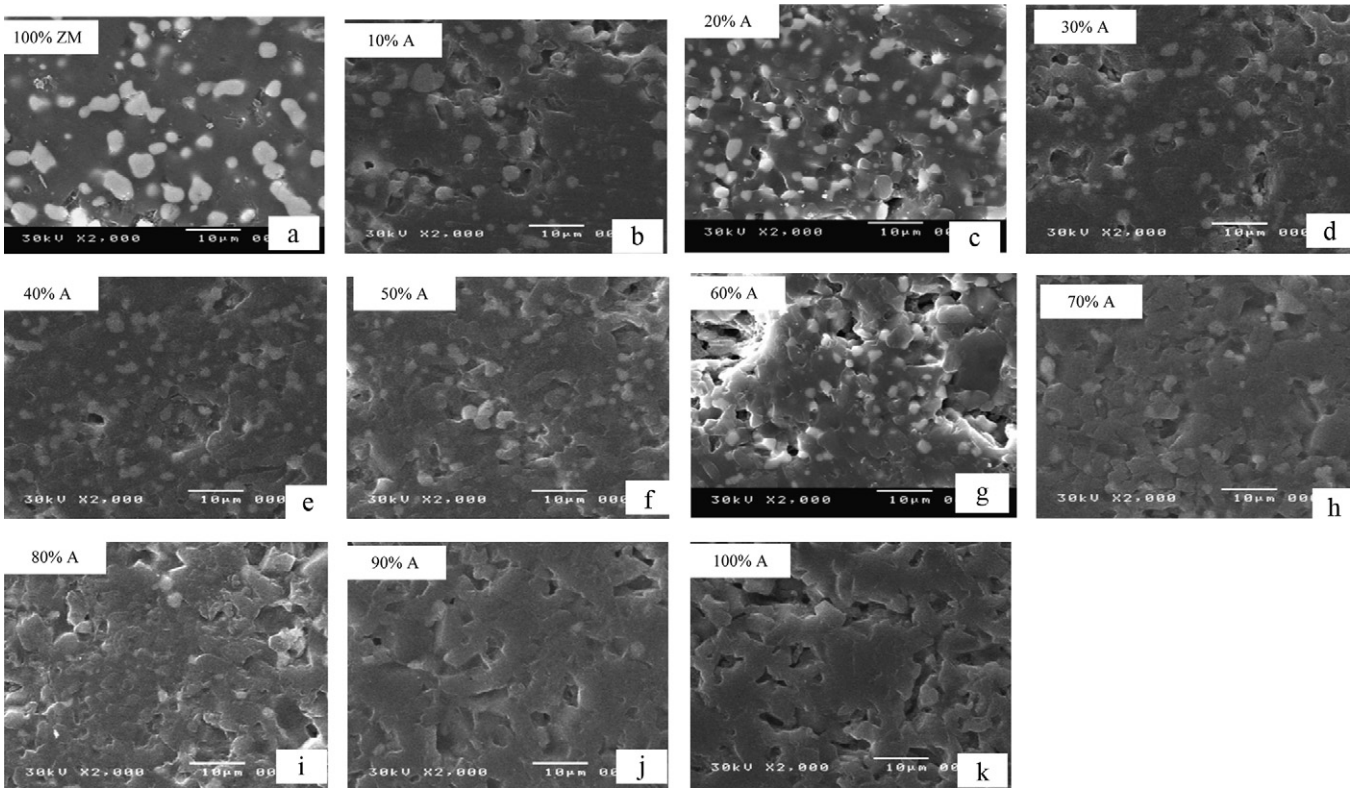

Fig. 5. Microstructure of separated ZM/A composites from 100% ZM (a) to 100% A (k) layer.

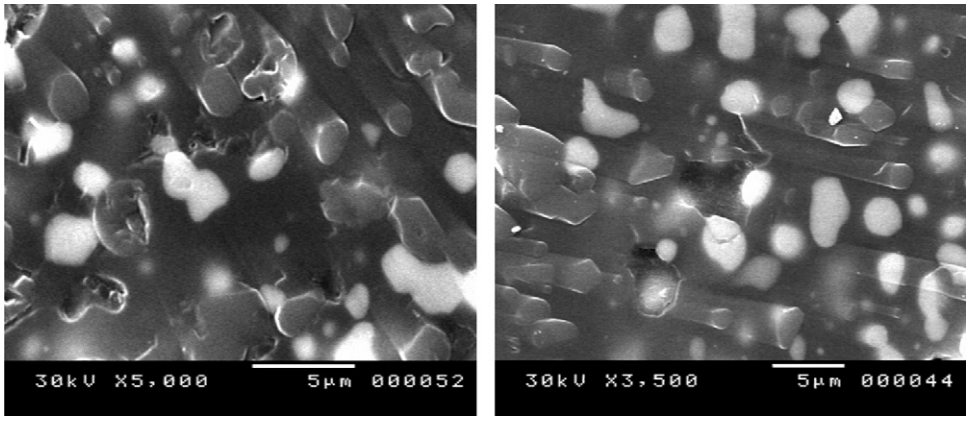

Fig. 6. Elongated grains of alumina.

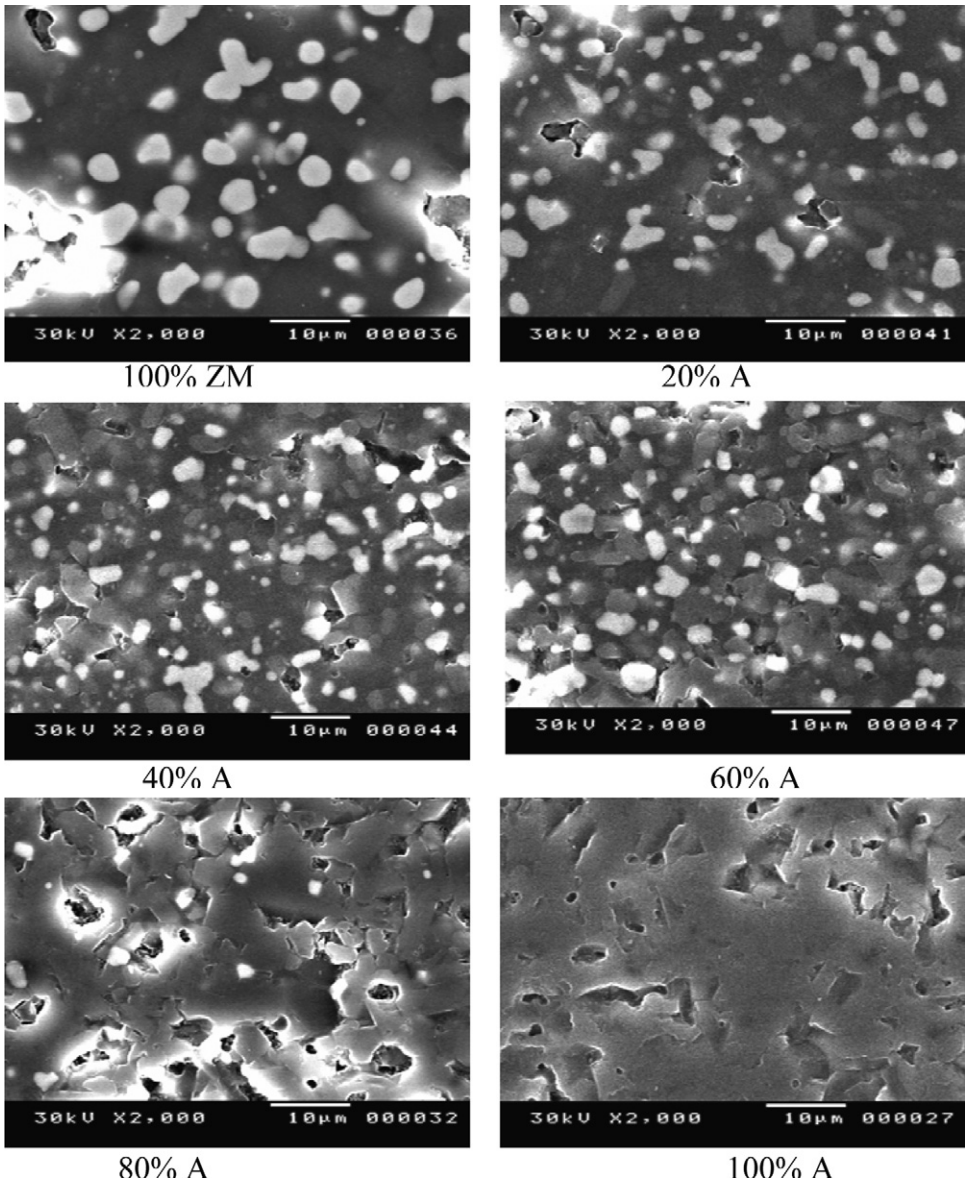

Fig. 7. Microstructure graded profile of the FGZM/A at different positions.

variation in zirconia, mullite and alumina contents from composite 1–11. The white grains are zirconia while gray and dark gray grains are alumina and mullite respectively. Generally, the matrix for all composites shows a homogeneous distribution of zirconia, mullite and alumina. There is a small level in porosity ranging between 1.0 and 10%, meaning that the liquid phase formed is not enough to form fully dense structure. Two types of zirconia grains are indicated. The first type is intragranular rounded ZrO_2 particle impeded in the mullite grains; this type is especially observed in composites with higher zirconia concentration. The second one is intergranular ZrO_2 particles with sharp edges located between mullite grains as observed.[14,24,26,61] The different shapes of ZrO_2 can be attributed to the densification behavior and phase evolution. The presence of spherical ZrO_2 grains (intragranular) refers to the growth in non-crystalline phases (amorphous silica) resulting from the dissociation of zircon to zirconia and silica and most likely in the liquid phase.[62–64] Some intergranular ZrO_2/ZrO_2 grains are so closed to each other and form long necks (coalescence of adjacent ZrO_2) and consequently changed into one grain (grain growth). This coalescence of ZrO_2 grains indicates that the sintering (densification) conditions employed (1650 °C/6 h) is enough to reach sintering and promoted the zirconia grain growth. The coarsening of intergranular ZrO_2 grains is decreased by increasing the amount of alumina in matrix as observed starting from composite 7 (60% alumina) as the high alumina content constrain and retard the growth of ZrO_2 grains.[27,65] Alumina crystals show a tendency to be elongated in the presence of high silica content and appear as randomly oriented rod like shapes as observed in Fig. 6. This can be explained as following; during the zircon dissociation into ZrO_2 and SiO_2, alumina particles started to dissolve in the SiO_2 phase region and formed mullite grains, while excess alumina is randomly oriented in rod like crystals.[66,67] So, this behavior of alumina only appears in composites with higher zircon content.

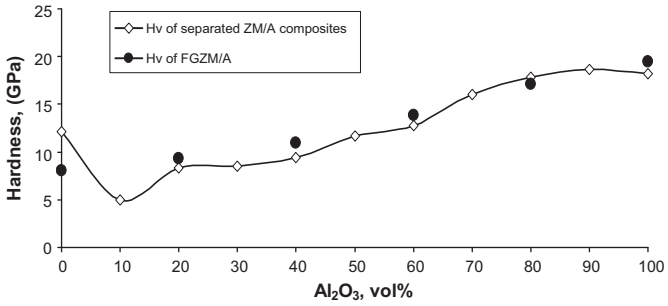

Fig. 8. Vickers hardness (GPa) of the different ZM/A composites and FGZM/A as a function of alumina vol%.

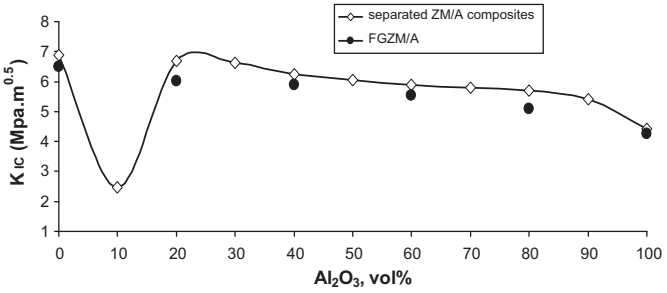

Fig. 9. Fracture toughness (K_{IC}) of the different ZM/A composites and FGZM/A as a function of alumina vol%.

The microstructure graded profile of the functionally graded zirconia–mullite/alumina at six different positions from zirconia–mullite side to alumina side is illustrated in Fig. 7. It shows the similar microstructure observations and grains morphology of its separated composites. There is a noticeable graded change in composition of zirconia, mullite and alumina from zirconia–mullite side to the alumina rich side of the FGZM/A structure.

3.2.3. Mechanical properties

3.2.3.1. Hardness. Hardness of the reaction sintered non-layered ZM/A composites as a function of alumina vol% measured by Vickers indentation at applied load of 30 kg is shown in Fig. 8. With the increase of alumina vol% from 10% to 100% the hardness value of the different composites increases gradually to reach its maximum at 90% alumina composite. This behavior can be attributed to the decrease of porosity and the increase of bulk density. The highest hardness values measured was around 17.659 GPa for composite involved 90% alumina and then decreased to 17.021 GPa for pure alumina layer. These values are in a good agreement with densification behavior of these composites and the reported data for pure alumina.[66,68] The lowest value was around 4.27 GPa for composite involved 10% alumina. This is attributed to its high porosity and low density. 100% zirconia–mullite composite has hardness value of 12.159 GPa. This value meets reported data.[27,69]

For FGZM/A, different hardness measurements were taken at six positions from ZM external layer to pure alumina layer in order to provide a gradient profile in its properties as recorded in Table 5 and Fig. 8. Hardness of FGZM/A showed a gradient in its values from ZM side to alumina side and match with values of its individual composite layers. This reflects the high dense, fine grained matrix and homogeneous distribution of the different layers through the tailored FGZM/A.

Table 5
Hardness profile distribution of the FGZM/A at different positions.

Measured positions	Position from ZM side (mm)	Layer composition
1	0.90	100%ZM
2	2.44	80%ZM/20%A
3	4.89	60%ZM/40%A
4	7.35	40%ZM/60%A
5	9.90	20%ZM/80%A
6	11.65	100%A

3.2.3.2. Fracture toughness. The crack pattern result values developed from indentation fracture at applied load of 30 kg for the individual ZM/A composite layers gave two crack patterns, palmquist and half penny. All the individual ZM/A composite layers gave palmquist crack type except composites contained 10, 90 and 100% alumina gave half-penny crack type. By applying the indentation fracture equations on both crack types for different composites, the fracture toughness (K_{IC}) of the reaction sintered composites increased gradually by the increase of zirconia content and the decrease of alumina content as shown in Fig. 9. ZM composite recorded the maximum K_{IC} value (6.52 Mpa $m^{0.5}$) while by increasing alumina from 10% to 100%, K_{IC} values decreased gradually to reach to 3.72 Mpa $m^{0.5}$ for pure alumina. The fracture toughness of 10% alumina composite is considered low due to the large amount of porosity present in this composite. Expected K_{IC} value based chemical composition of the individual composite layers assuming that the crack propagates in a straight manner must equal ~2.6 Mpa $m^{0.5}$ [70] which is considered much lower than the measured values (~2.5–6.5 Mpa $m^{0.5}$). The increase of K_{IC} can be attributed to the transformation of zirconia from tetragonal to monoclinic under cooling from sintering temperature to room temperature.[14,66,71–76] The presence of elongated grains of alumina as seen by SEM deflects the propagation of cracks and improves the fracture toughness as well.[66,67] Also, thermal expansion mismatch among the composite phases (alumina = 8.2×10^{-6} K^{-1}, mullite = 5.1×10^{-6} K^{-1} and 7.6×10^{-6} K^{-1} for zirconia) develops desirable microcracks and in turn enhances K_{IC} value.[31,39,77,78]

K_{IC} values and crack types of the FGZM/A measured at different positions exhibited quite similarity in crack types and K_{IC} values trends of the individual composites layers as shown in Fig. 9. These results reflect the added value of the highest strength of the formed interfacial bonding among the layers of the tailored FGZM/A.

3.2.3.3. Cold crushing strength. The cold crushing strengths of the FGZM/A and its non-layered composites is shown in Fig. 10. It is noted that a gradual increase in the CCS with the increase of the amount of alumina added from 10 to 90 vol% and then decreased in last layer (100% alumina). The maximum value of

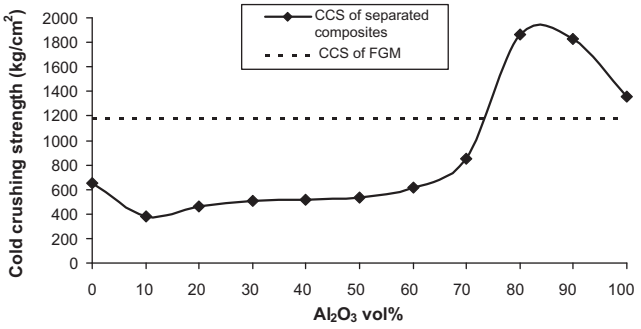

Fig. 10. Cold crushing strength of FGZM/A and the different ZM/A composites as a function of alumina vol%.

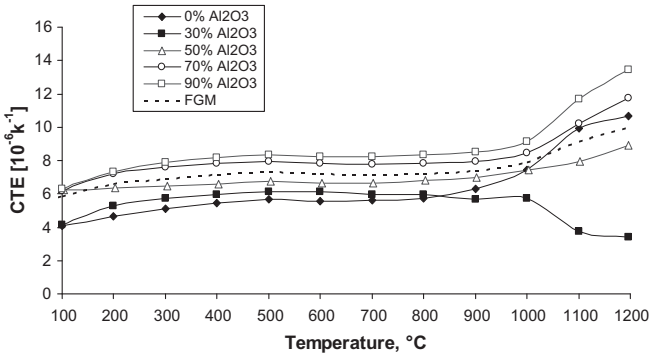

Fig. 12. CTE of FGZM/A and different composites as a function of temperature.

CCS recorded is 1861.7 kg/cm^2 for non-layered composite containing 90% alumina and the minimum value is 381.8 kg/cm^2 for 10% alumina. ZM composite gave the highest CCS value compared by the others. These results are in good agreement with densification responses and hardness trends of the sintered samples. This correlation can be supported by flows in ceramics where presence of cracks and pores has large effect in reducing the CCS values.[23,72,79] The recorded CCS value of the FGZM/A (1178.128 kg/cm^2) is significantly higher than the average value of its non-layered composites (869.8 kg/cm^2). This remarkable enhancement in CCS values gives an indication of strong interfacial bonding between each two adjacent layers and confirms the success to obtain a continuous and homogenous FGZM/A structure without sharp interfaces.

3.2.4. Thermal properties

3.2.4.1. Thermal expansion. Linear thermal expansion (LTE) and its coefficient (CTE) of FGZM/A and some selected non-layered composites as a function of temperature are shown in Figs. 11 and 12. It is obvious that LTE and CTE of non-layered composites are linearly increased with the increase of the temperature from 100 to 1100 °C. In this range of temperature (up to 1100 °C), the most of LTE and CTE values of these composites recorded gradual increase with the increase of alumina content. Such kind of LTE and CTE increases can be realized from the high LTE of alumina reported when compared to zirconia and mullite.[31,39,77,78] LTE and CTE of these systems increase with the increase of temperature up to 1000 °C can be understood based on literature.[80] However, a deviation from linear trend of LTE and CTE took place with increasing the temperature above 1000 °C, This might be caused by ZrO_2 inversion from monoclinic to tetragonal according to the following equation[81]:

$$\text{m-}ZrO_2 \underset{\sim 950\,^\circ\text{C}}{\overset{1170\,^\circ\text{C}}{\rightleftarrows}} \text{t-}ZrO_2 \overset{2370\,^\circ\text{C}}{\leftrightarrow} \text{c-}ZrO_2 \overset{2706\,^\circ\text{C}}{\leftrightarrow} \text{melt}$$

This transformation or inversion of the formed ZrO_2 is likely martensitic in nature. It is termed as "brittle-martensite" transformation.[14,66,71–76] It has generated great interest among scientists, technologists, and users, because it contributes to the toughening enhancement of ceramics. CTE of ZM (100%) and alumina (100%) recorded are $5.4 \times 10^{-6}\,^\circ\text{C}^{-1}$ and $7.83 \times 10^{-6}\,^\circ\text{C}^{-1}$ respectively. These values confirm the presence of mismatch in thermal expansion between zirconia–mullite and alumina layers. On the other hand, LTE and CTE of FGZM/A recorded are approximately the average values of all its non-layered composites. This means that it is possible to control the thermal properties of tailored multilayered composite by increase or decrease LTE or CTE based on the properties of the its single layers.

3.2.4.2. Thermal shock resistance. The macrohardness distribution of the reaction sintered ZM/A composites before and after successful 30 heating/water quenching cycles without spalling or crumbling are shown in Fig. 13. The recorded data revealed that all non-layered composites and FGZM/A subjected to 30 subsequent thermal shock cycles have lower values compared by the unexposed one to thermal shock. This reduction is due to the softening of the matrix caused by the thermal exposure. ZM

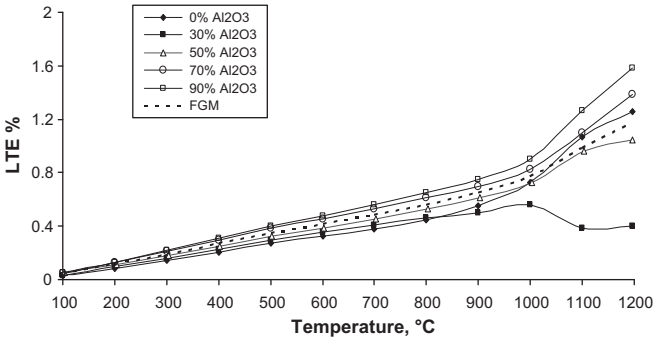

Fig. 11. LTE of FGZM/A and different composites as a function of temperature.

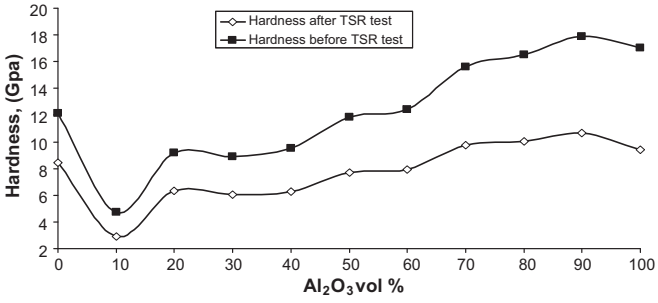

Fig. 13. Hardness distribution of ZM/A composites as a function of alumina vol% before and after 30 thermal shock cycles.

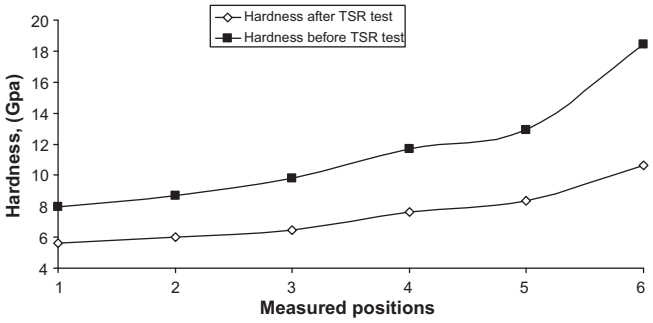

Fig. 14. Hardness distribution of the FGZM/A at different positions before and after 30 thermal shock cycles.

composite gave 30 cycles with retention of ∼70% of its original hardness. With the decrease of mullite and zirconia contents, the retention percent decreases gradually up to less than 55% of its original value for alumina layer. This trend is attributed to several factors. Firstly, thermal shock resistance (TSR) increases if the phases constitute the structure of the object has low thermal expansion coefficient and Young's modulus or high thermal stress.[82] TSR value of mullite is high compared to those of engineering materials, such as Al_2O_3, SiO_2 and Si_3N_4.[23] Therefore, the formation of mullite and increasing its content contribute to enhancement of the resistance to thermal shock. In addition, mullite has a softening nature (thermoelastic behavior) because of its low thermal expansion.[83] Thus the formed composites have good ductility. Secondly, TSR can be increased by increasing the toughening mechanism and inhibiting the crack propagation. Zirconia plays the most important role in increasing the toughness value due to its transformation toughening effect and its capability to restrict the crack propagation to short distance through the material. In addition, the generation of fine intergranular cracks caused by anisotropic thermal expansion properties of the structure phases during the subsequent thermal shock cycles absorbs the strain energy during the cycles, which, consequently, enhances TSR. Therefore, the formation of zirconia and increasing its content contribute to enhancement

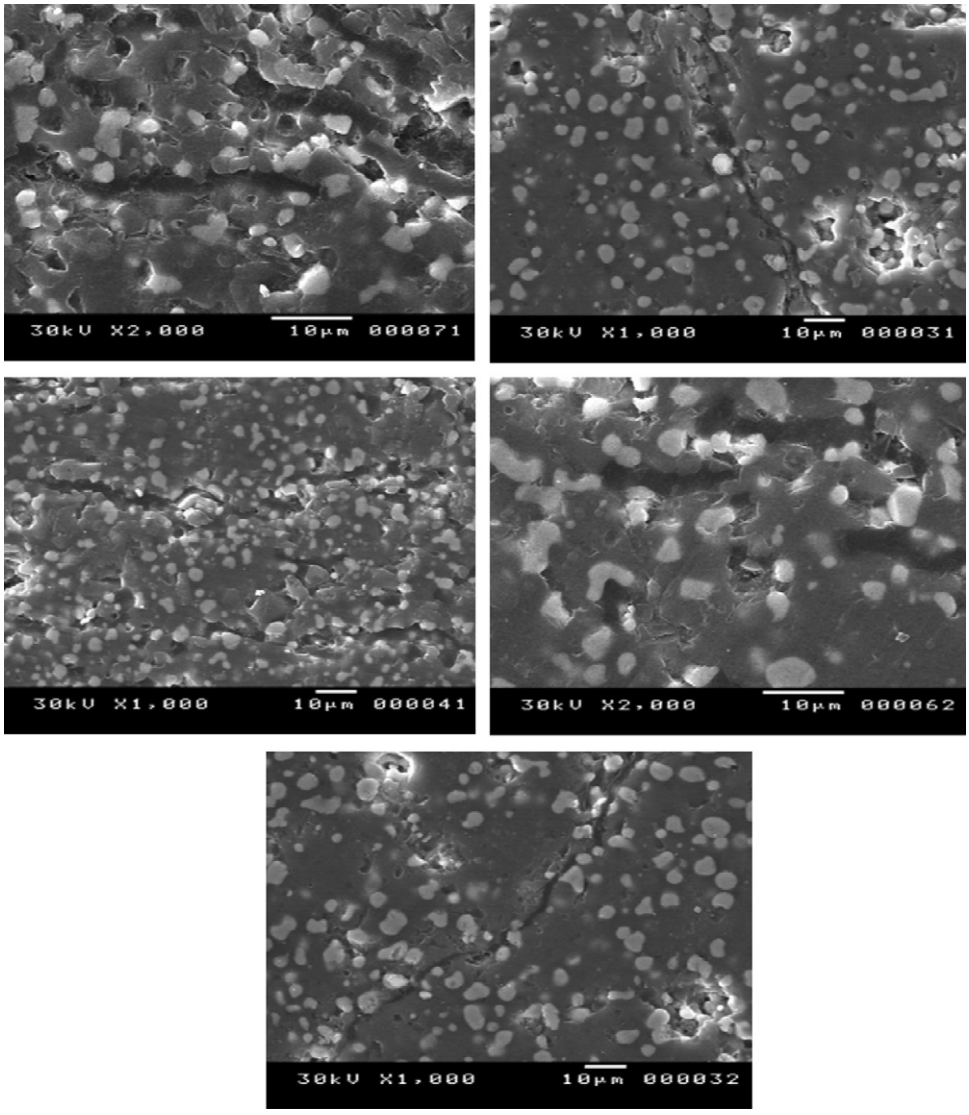

Fig. 15. Photographs of cracks in different ZM/A composites subjected to 30 thermal shock cycles.

of the resistance to thermal shock. Based these factors mentioned and the reported data,[31,39,61,67,84,85] the introduction of mullite and zirconia into alumina ceramics in this work led to remarkable enhancement in the thermal shock behavior. A gradient in the macrohardness of FGZM/A was recorded at different positions starting from ZM side to alumina side before and after subsequent 30 thermal shock cycles as shown in Fig. 14. In addition, quite similar macrohardness trend between FGZM/A and its non-layered composites was noted. There is no degradation or de-laminations of the FGZM/A layers are observed.

Despite the subjection of ZM/A composites to 30 subsequent thermal shock cycles, no noticeable change in the microstructure was seen as shown in Fig. 15. However, thermal shocks caused permanent damages in the form of crack. This crack undergoes intergranular fracture mode and does not propagate in straight line. It moves across alumina/mullite grain boundaries and does not affect on zirconia grains. Also, it is obvious that the crack on the surface has wavy nature and does not propagate sharply to the edges of the samples. It is arrested by some pores formed and zirconia grains. This microstructure feature is considered as advantage for the properties of tailored FGZM/A from its non-layered composites.

4. Conclusions

Continuous functionally graded zirconia–mullite/alumina has been successfully tailored by reaction sintering of alumina and zircon. The studied parameters (different alumina particle sizes, sintering temperatures and times) showed a strong effect on the reaction response and densification behaviors. It was found that, decreasing alumina particle size to 2.5 μm, increasing sintering temperature to 1650 °C and sintering time to 6 h gave complete reaction and the highest densification level in the different non-layered composites and the graded structure. The functionally graded zirconia–mullite/alumina gave 5.24% apparent porosity, 3.451 g/cm^3 bulk density and 17.22% linear shrinkage based on these conditions. Increasing hardness (Hv) values for different zirconia–mullite/alumina composites recorded were correlated by the increase of the bulk density and alumina vol%. The increase of the fracture toughness (K_{IC}) values were understood in terms of the presence of small amounts of pores, elongated grains, small mismatch of the CTE between different phases and ZrO_2 toughening mechanisms. Cold crushing strength (CCS) of the different samples increased with increasing their densification levels and alumina vol%. Thermal shock resistance (TSR) of the reaction sintered ZM/A composites and tailored FGZM/A increased with increasing zirconia and mullite contents. The cracks generated from thermal shock test did not propagate to the edges of the samples and arrested by zirconia grains and some pores formed. Functionally graded zirconia–mullite/alumina showed a gradient in its properties from one layer to the other and gave a homogenous structure with highly improved physical, mechanical and thermal properties. The different properties of tailored FGZM/A recorded average values or rather better of its non-layered composites which reflected the strong interfacial bonding and homogenous distribution of powders in its different layers. It is possible to tailor FGZM/A with controlled properties based on the properties of non-layered ZM/A composites. The successful tailored FGZM/A can be nominated to be used in refractory and high temperature applications.

References

1. Kaya C. Al_2O_3–Y–TZP/Al_2O_3 functionally graded composites of tubular shape from nano-sols using double-step electrophpretic deposition. *J Eur Ceram Soc* 2003;**23**:1655–60.
2. Cannillo V, Manfredini T, Siligardi C, Sola A. Preparation and experimental characterization of glass–alumina functionally graded materials. *J Eur Ceram Soc* 2006;**26**(6):993–1001.
3. Leong KF, Chuna CK, Sudaramadji N, Yeong WY. Engineering functionally graded tissue engineering scaffolds. *J Mech Behav Biomed Mater* 2008;**1**:140–52.
4. Limarga AM, Widjaja S, Yip TH. Mechanical properties and oxidation resistance of plasma-sprayed multilayered Al_2O_3/ZrO_2 thermal barrier coatings. *Surf Coat Technol* 2005;**197**:93–102.
5. Paszkiewicz B, Paszkiewicz R, Wosko M, Radziewicz D, Sciana B, Szyszka A, Macherzynski W, Tlaczla M. Functionally graded semiconductor layers for device applications. *J Surf Eng Surf Instrum Vacuum Technol* 2008;**82**:389–94.
6. Petrovic JJ, McClellan KJ. *Ceramic/polymer functionally graded material (FGM) lightweight armor system*. DOE Office of Scientific and Technical Information (OSTI); 1997, 96510.
7. Vasileèv AD, Akimav GYa, Kaval AYu. Zirconium ceramics and its future prospects in Ukraine. *Refract Ind Ceram* 2000;**41**(9–10):235–7.
8. Lin Y, Chen Y. Fabrication of mullite composites by cyclic infiltration and reaction sintering. *Mater Sci Eng* 2001;**A298**:179–86.
9. Zhao SK, Huang Y, Wang C, Huang X, Guo J. Mullite formation from reaction sintering of $ZrSiO_4$/αAl_2O_3 mixtures, Part A. *Mater Lett* 2003;**57**:1716–22.
10. Li DX, Thompson WJ. Kinetic mechanisms for mullite formation from sol–gel precursors. *J Mater Res* 1990;**5**(9):1963–9.
11. Anikumar GM, Hareesh US, Damodaran AD, Warriers KGK. Effect of seeds on the formation of sol–gel mullite. *Ceram Int* 1997;**23**(6):537–43.
12. Dokko PC, Pask JA, Mazdixasni KS. High-temperature mechanical properties of mullite under compression. *J Am Ceram Soc* 1977;**60**(3–4):150–5.
13. Zhao SK, Huang Y, Wang CA. Sinterability of $ZrSiO_4$/αAl_2O_3 mixed powders, Part B. *Ceram Int* 2003;**29**:49–53.
14. Mazzei AC, Rodrigues JA. Alumina–mullite–zirconia composites obtained by reaction sintering, Part I: Microstructure and mechanical behavior. *J Mater Sci* 2000;**35**:2807–14.
15. Zanatto ED, Migliore AR. Propriedades mecânicas de materiais cerâmicos: uma introducâo. *Cerâmica* 1991;**37**:247.
16. Evans AG, Cannon RM. Toughening of brittle solids by martensitic transformations. *Acta Metall* 1986;**34**(5):761.
17. Nakamura T. Novel zirconia/alumina composites for TJR. *Key Eng Mater* 2003;**240–242**:765–8.
18. Begand S, Oberbach T, Glien W. Tribological behaviour of an alumina toughened zirconia ceramic for an application in joint prostheses. *Key Eng Mater* 2006;**309–311**:1261–4.
19. Oberbach T, Ortmann C, Begand S, Glien W. Investigations of an alumina ceramic with zirconia gradient for the application as load bearing implant for joint prostheses. *Key Eng Mater* 2006;**309–311**:1247–50.
20. Boniecki M, Librant Z, Tomaszewski H. Fracture toughness and strength of Al_2O_3–ZrO_2 nanocomposites. *Key Eng Mater* 2002;**223**:209–14.
21. Kim D-J, Han J-S, Lee S-H, Yang J-H. Zirconia–alumina composite dental implant abutments. *Key Eng Mater* 2004;**254–256**:699–702.
22. Mitra BL, Biswas NC, Aggarwal PS. Zirconia–mullite ceramics by reaction-sintering. *Bull Mater Sci* 1989;**12**(5):457–60.
23. Ewais EMM. Sintering response of in situ zirconia/mullite ceramic composite. *Am Ceram Soc Bull* 2007;**86**(12):9101–10.
24. Orange G, Fantozzi G. High temperature mechanical properties of reaction-sintered mullite/zirconia and mullite/alumina/zirconia composites. *J Mater Sci* 1985;**20**:2533–40.

25. Pena P, Moya JS, Aza SD. Effect of magnesia additions on the reaction sintering of zircon/alumina mixtures to produce zirconia toughened mullite. *J Mater Sci Lett* 1983;**2**:772–4.
26. Miranzo P, Pena P, Aza S, Moya JS. TEM study of reaction-sintered zirconia–mullite composites with CaO and MgO additions. *J Mater Sci* 1987;**22**:2987–92.
27. Garrido LB, Aglietti EF, Martorello L, Camerucci MA, Cavalieri AL. Hardness and fracture toughness of mullite–zirconia composites obtained by slip casting. *J Mater Sci Eng A* 2006;**419**:290–6.
28. Quan LS, Jie Z, Xiao-ping T, Yan T. Mechanical properties and structure of zirconia–mullite ceramics prepared by in situ controlled crystallisation of Si–Al–Zr–O amorphous bulk. *Trans Nonferrous Met Soc China* 2008;**18**:799–803.
29. Ozturk C, Tur YK. Processing and mechanical properties of textured mullite/zirconia composites. *J Eur Ceram Soc* 2007;**27**:1463–7.
30. Aksel C, Konieczny F. Mechanical properties and thermal shock behaviour of psr-333 alumina–mullite–zirconia refractory material. *Glass Int* 2001;**24**(1):16–8.
31. Aksel C. Mechanical properties and thermal shock behaviour of alumina–mullite–zirconia and alumina–mullite refractory materials by slip casting, Part B. *Ceram Int* 2003;**29**:311–6.
32. Parkinson DE. Feeder and forehearth refractories. *Glass Technol* 1988;**29**(5):173–6.
33. Medvedovski E. Wear-resistant alumina ceramics. *Int Ceram* 2000;**49**(2):106–13.
34. Medvedovski E. Armor alumina ceramics. In: McCauley JW, Crowson A, Gooch Jr WA, et al., editors. *Ceramic transactions, vol. 134, ceramic armor materials by design*. Westerville, OH: American Ceramic Society; 2002. p. 91–101.
35. Medvedovski E. Alumina–mullite ceramics for structural applications. *Ceram Int* 2006;**32**:369–75.
36. Taktak S, Baspinar MS. Wear and friction behaviour of alumina/mullite composite by sol–gel infiltration technique. *Mater Design* 2005;**26**(5): 459–64.
37. Manfredo LJ, Mcnally RN. The corrosion resistance of high ZrO_2-fusion cast Al_2O_3–ZrO_2–SiO_2 glass refractories in soda lime glass. *J Mater Sci* 1984;**19**(4):1272–6.
38. Asokan T. Microstructural features of fusion cast Al_2O_3–ZrO_2–SiO_2 refractories. *J Mater Sci Lett* 1994;**13**:343–5.
39. Aksel C. The influence of zircon on the mechanical properties and thermal shock behavior of slip-cast alumina–mullite refractories. *Mater Lett* 2002;**57**(4):992–7.
40. ASTM, C373-72: Test method for water absorption, bulk density, apparent porosity and apparent specific gravity of white ware products, annual book of ASTM, vol. 15, USA; 1984.
41. ASTM C1327-03: Test method for Vickers indentation hardness of advanced ceramics, Annual book of ASTM standards, Section 15, vol. 15.01. West Conshohocken, PA: ASTM; 2006.
42. Sergejev F, Antonov M. Comparative study on indentation fracture toughness measurements of cemented carbides. *Proc Estonian Acad Sci Eng* 2006;**12**:388–98.
43. Bamzai KK, Kotru PN, Wanklyn BM. Investigations on indentation induced hardness and fracture mechanism in flux grown DyAlO crystals. *Appl Surf Sci* 1998;**133**:195–204.
44. Yount HJ. Hardness and fracture toughness of heat treated advanced ceramic materials for use as fuel coating and inert matrix materials in advanced reactors, M.Sc. Thesis, University of Wisconsin Madison; 2006.
45. Lawn HR, Fuller ER. Equilibrium penny-like cracks in indentation fracture. *J Mater Sci* 1975;**10**:2016–24.
46. Sevim I, Kulekci MK. Abrasive wear behaviour of bio-active glass ceramics containing apatite. *Bull Mater Sci* 2006;**29**:243–9.
47. Miyazaki H, Hyuga H, Hirao K, Ohji T. Comparison of fracture resistance as measured by the indentation fracture method and fracture toughness determined by the single edge-precracked beam technique using silicon nitrides with different microstructures. *J Eur Ceram Soc* 2007;**27**(6):2347–54.
48. Mukhopadhyay A, Basu BS, Bakshi Das, Mishra SK. Pressureless sintering of ZrO_2–ZrB_2 composites: microstructure and properties. *Int J Refract Met Hard Mater* 2007;**25**:179–88.
49. Albakry M, Guazzato M, Swain MV. Fracture toughness and hardness evaluation of three pressable all-ceramic dental materials. *J Dent* 2003;**31**: 181–8.
50. Ewais EMM, Attia MAA, Abousree-Hegazy A, Bordia RK. Investigation of the effect of ZrO_2 and ZrO_2/Al_2O_3 additions on the hot-pressing and properties of equimolecular mixtures of α- and β-Si_3N_4. *Ceram Int* 2010;**36**(4):1327–38.
51. Keryvin V, Hoang VH, Shen J. Hardness, toughness, brittleness and cracking systems in an iron-based bulk metallic glass by indentation. *J Intermetallics* 2009;**17**:211–7.
52. Curkovic L, Rede V, Grilec K, Mulabdic A. Hardness and fracture toughness of alumina ceramics. In: *12. Conference on materials, processes, friction and wear*. 2007.
53. Dietz M, Tietz H-D. Characterization of engineering ceramics by indentation methods. *J Mater Sci* 1990;**25**:3731–8.
54. ASTM, C1424-04: Test method for cold crushing strength of advanced ceramics, annual book of standards, section 15, vol. 15.01; 2006.
55. ASTM, C372-94: Test method for linear thermal expansion of porcelain, enamel and glaze frits and fired ceramic white ware products by the dilatometer method, annual book of standard, vol. 15; 2001.
56. Determination of resistance to thermal shock, Part I – Water quenching. *PRE/R5*; 1987;**1**(III26):1–2.
57. Rupo E, Gilbart E, Carruthers TG, Brook RJ. Reaction hot pressing of zircon–alumina mixtures. *J Mater Sci* 1979;**14**(3):705–11.
58. Claussen N, Jahn J. Mechanical properties of sintered in situ reacted mullite–zirconia composites. *J Am Ceram Soc* 1980;**63**(3–4):228–9.
59. Dörre E, Hübner H. *Alumina-processing, properties and applications*. Springer-Verlag; 1984.
60. Bhattacharyya M, Kumar AN, Kapuria S. Synthesis and characterization of Al/SiC and Ni/Al_2O_3 functionally graded materials. *J Mater Sci Eng A* 2008;**487**:524–35.
61. Rendtorff NM, Garrido LB, Aglietti E. Mullite-zirconia–zircon composites: properties and thermal shock resistance. *Ceram Int* 2009;**35**: 779–86.
62. MeCartney ML. Influence of an amorphous second phase on the properties of yttria stabilized tetragonal polycrystals (Y-TZP). *J Am Ceram Soc* 1987;**70**(1):54–8.
63. Cambier F, Delalastra CB, Pilate P, Leriche A. Formation of microstructural defects in mullite–zirconia and mullite–alumina–zirconia composites obtained by reaction-sintering of mixed powders. *Trans J Br Ceram Soc* 1984;**83**(6):196–200.
64. Wallace JS, Petzow G, Claussen N. Advance in ceramics, science and technology of zirconia II. *Am Ceram Soc* 1983;**12**:436. Columbus, OH.
65. Zao S-K, Huang Y, Wang C-A, Huang X-X, Guo J-K. Sinterability of ZrSiOVa–AliOs mixed powders. *Ceram Int* 2003;**29**:49.
66. Casellas D, Nagl MM, Lianes L, Anglada M. Fracture toughness of alumina and ZTA ceramics: microstructural coarsening effects. *J Mater Process Technol* 2003;**143–144**:148–52.
67. Aksel C. The microstructural features of an alumina–mullite–zirconia refractory material corroded by molten glass, Part A. *Ceram Int* 2003;**29**:305–9.
68. Morrell R. *Handbook of properties of technical and engineering ceramics, Part 1*. London: HMSO; 1985.
69. Richerson DW. *Modern ceramic engineering, properties, processing and use in design*. New York/Basel: Marcel Dekker; 1982. p. 85.
70. Baudin C, Cambier F, Delaey L. Fractographic study of the alumina and zirconia particles embedded in mullite prepared by reaction sintering. *J Mater Sci* 1986;**21**:4024–8.
71. Basu B. Toughening of yttria-stabilized tetragonal zirconia ceramics. *Int Mater Review* 2005;**50**(239):256.
72. Bengisu M. *Engineering ceramics*; 2001. Berlin, Germany. p. 28–30, 358, 407–44.
73. Becher PF, Alexander KB, Warmick W. Influence of ZrO_2 grain size and content on the transformation response in the Al_2O_3–ZrO_2 (12 mol% CeO_2) System. *J Am Ceram Soc* 1993;**76**:657.
74. Karihaloo BL. Contributions of t-m phase transformation to the toughening of ZTA. *J Am Ceram Soc* 1991;**74**:1703.

75. Evans AG. Perspective on the development of high toughness ceramics. *J Am Ceram Soc* 1990;**73**:187.
76. Green DJ, Hannink RHJ, Swain MV. *Transformation toughening of ceramics*. Boca Raton, FL: CRC Press; 1989.
77. Shackelford JF, Alexander W, Park JS. *CRC materials science and engineering handbook*. Boca Raton, FL: CRC Press; 1994.
78. Burnett SJ. *Properties of refractory materials*; 1969. UKAEA, Research Group Report, Harwell.
79. Richerson DW. *Modern ceramic engineering properties, processing and use in design*. 3rd ed; 2006. USA.
80. Schneider H, Okada K, Pask JA. *Mullite and mullite ceramics*. New York: Wiley; 1994. p. 224.
81. Yoshimura M. Phase stability of zirconia. *Am Ceram Soc Bull* 1988;**67**(12):1950–5.
82. Achari S, Satapathy LN. Mullite based refractories for molten-metal application. *J Am Ceram Soc Bull* 2003;**82**(3):1–6.
83. Reddy NK. Reaction-bonded silicon carbide refractories. *Mater Chem Phys* 2002;**76**:78–81.
84. Rendtorff NM, Garrido LB, Aglietti EF. Thermal shock behavior of dense mullite–zirconia composites obtained by two processing routes. *Ceram Int* 2008;**34**:2017–24.
85. Zender H, Leistner H, Searle H. ZrO_2 materials for applications in the ceramic industry. *Interceramics* 1990;**39**(6):33–6.